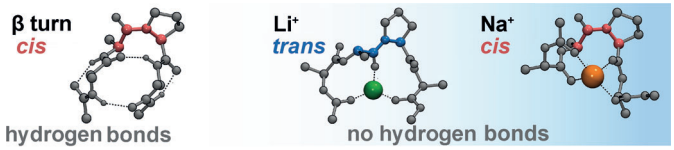

Traffic lights for protein folding: The structure of peptides and proteins is strongly influenced by specific interactions between metal ions and the backbone. A combination of density-functional theory and gas-phase spectroscopy show that coordination of Li and Na cations can break the local hydrogen-bonding network and induce considerably different prolyl peptide bond conformations in the same model peptide (see picture).

Protein Folding

C. Baldauf, K. Pagel,* S. Warnke, G. von Helden, B. Koksch, V. Blum,* M. Scheffler* ..... ▮▮▮▮–▮▮▮▮

How Cations Change Peptide Structure

CHEMISTRY
A EUROPEAN JOURNAL

ChemPubSoc
Europe

DOI: 10.1002/chem.201204554

How Cations Change Peptide Structure

Carsten Baldauf,*[a] Kevin Pagel,*[a] Stephan Warnke,[a] Gert von Helden,[a] Beate Koksch,[b] Volker Blum,*[a] and Matthias Scheffler[a]

Abstract: Specific interactions between cations and proteins have a strong impact on peptide and protein structure. Herein, we shed light on the nature of the underlying interactions, especially regarding effects on the polyamide backbone structure. This was done by comparing the conformational ensembles of model peptides in isolation and in the presence of either Li^+ or Na^+ by using state-of-the-art density-functional theory (including van der Waals effects) and gas-phase infrared spectroscopy. These monovalent cations have a drastic effect on the local backbone conformation of turn-forming peptides, by disruption of the hydrogen-bonding networks, thus resulting in severe distortion of the backbone conformations. In fact, Li^+ and Na^+ can even have different conformational effects on the same peptide. We also assess the predictive power of current approximate density functionals for peptide–cation systems and compare to results with those of established protein force fields as well as high-level quantum chemistry calculations (CCSD(T)).

Keywords: density-functional calculations · hydrogen bonds · IR spectroscopy · protein folding · protein structures

Introduction

As early as 1912, Paul Pfeiffer systematically studied the crystallization of short Ala-and Gly-containing peptides from aqueous solution in the presence of alkali salts[1] and postulated that Li^+ exhibits a higher affinity ("Additionsfähigkeit") for peptides than Na^+ and K^+.[2] Indeed, calorimetric studies revealed high interaction enthalpies for the interactions of a series of peptides with Li^+,[3] values that were in the range of solvation enthalpies of peptides. These strong interactions are in practice used to increase the proportion of *cis* prolyl peptide bonds from 10% to 70% through the addition of Li salts in biochemical activity assays of peptidyl prolyl *cis–trans* isomerases.[4] NMR studies of cyclic peptide cyclosporine A (CysA) in organic solvents revealed that Li^+ inhibits the formation of hydrogen bonds and induces unusual backbone conformations.[5,6] One hundred years after Pfeiffer's work, Garand et al.[7] studied the noncovalent interactions of a non-natural peptide-based catalyst by means of gas-phase infrared (IR) spectroscopy. When protonated, the polyamide backbone of the molecule forms intramolecular hydrogen bonds; however, when it is sodiated, there is an apparent complete absence of hydrogen bonds owing to the presence of interactions between the carbonyl groups and Na^+. Both CysA[5,6] and the peptide-based catalyst[7] form narrow turn-like backbone loops, which are well suited to accommodate a cation. Such turns are normally at the outside of globular proteins, where they are exposed to the surrounding medium. Herein, we investigate the atomistic and electronic basis of cation–peptide interactions in turn-forming peptides. The focus of the study is on proline-containing peptides, in which such interactions are expected to have pronounced conformational effects owing to the possible *cis* and *trans* states of the prolyl-peptide bond.[8] This study is based on accurate conformational predictions by using first principles (density-functional theory) in a synergistic combination with gas-phase IR spectroscopy to validate the results.

Structure formation and dynamics in proteins can be primarily attributed to the rotation of the $N–C_\alpha$ and $C_\alpha–C$ bonds, represented by the backbone torsion angles ϕ and ψ, respectively (Figure 1A). This conformational ϕ/ψ space is well described by a Ramachandran diagram,[9] which is used, for example, in the statistical evaluation of high-resolution X-ray data (Figure 1B).[10] The shaded areas are referred to as allowed conformational regions and can be associated with characteristic secondary structure types (Figure 1B).

[a] Dr. C. Baldauf, Dr. K. Pagel, Dipl.-Phys. S. Warnke, Dr. G. von Helden, Dr. V. Blum, Prof. Dr. M. Scheffler
Fritz-Haber-Institut der Max-Planck-Gesellschaft
Faradayweg 4-6, 14195 Berlin-Dahlem (Germany)
E-mail: baldauf@fhi-berlin.mpg.de
pagel@fhi-berlin.mpg.de
blum@fhi-berlin.mpg.de

[b] Prof. Dr. B. Koksch
Institut für Chemie und Biochemie - Organische Chemie
Freie Universität Berlin
Takustr. 3, 14195 Berlin-Dahlem (Germany)

Supporting information for this article contains details of the simulation setup, experimental procedures, energy hierarchies for AAPA+Li^+ geometries in the presence and absence of the respective cation at different levels of theory, backbone torsion angles of low-energy conformers of AAPA and ADPA in isolation and in the presence of Li^+ and Na^+, and Cartesian coordinates of the structures; this information is available on the WWW under http://dx.doi.org/10.1002/chem.201204554.

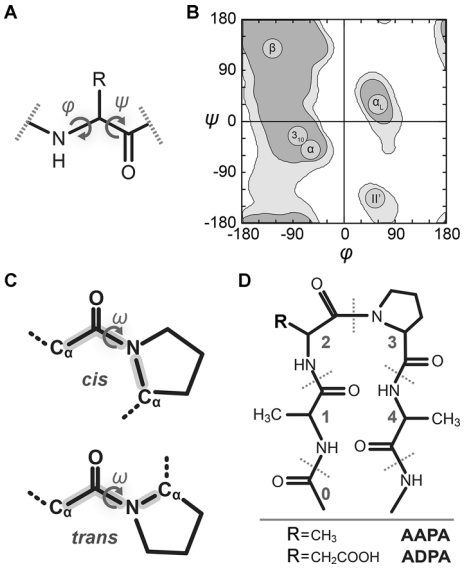

Figure 1. (A) The backbone torsion angles, φ and ψ, of the residues of a polypeptide chain. (B) Backbone torsion angles illustrated by a Ramachandran plot, based on data from ref. [10]; labels highlight characteristic secondary-structure types: the β region in the 2nd quadrant, the 3_{10} and the α-helical region in the 3rd quadrant, and the left-handed α and the βII' region in the 1st and 4th quadrants, respectively. (C) The *cis* and *trans* state of the prolyl-peptide bond. (D) The model peptides, AAPA and ADPA, shown in a schematic βVI-turn conformation.

The double-bond character of the peptide bond hinders free rotation and allows for two distinct conformations. In general, the *trans* conformation is almost exclusively observed with an apparent high barrier for its conversion into the *cis* form.[11,12] A significant fraction of *cis* conformation is only observed for the prolyl peptide bond.[13] In proline, the *cis* and *trans* forms (Figure 1C) are close in energy because the C_β of the preceding residue encounters a carbon atom of proline (C_α or C_δ) in both states. A *cis* peptide bond, usually preceding a proline residue, is a feature of so-called type β-VI turns (Figure 1D).[14,15] This notation dates back to work of Venkatachalam, according to which β turns share the feature of a hydrogen bond between residues $i+3$ and i and are further classified by the backbone torsion angles ϕ and ψ of the residues $i+1$ and $i+2$.[16] The β turns of the protein backbone allow for a 180° reversal of the direction of structure propagation within four consecutive residues of a polypeptide chain. Similarly, Hutchinson and Thornton classify β turns according to ranges of values for the backbone torsion angles ϕ and ψ, thus giving eight well-defined classes (I, I′, II, II′, VIa1, VIa2, VIb, and VIII) and a miscellaneous type IV.[17,18] Very prominent are the common (type I) and glycine (type II) turn and their inverse counterparts, I′ and II′. The special β-turn types VIa and VIb have a *cis* peptide bond between central residues $i+1$ and $i+2$; these β-turn types frequently feature proline in position $i+2$.[14,15]

In this study, we make use of the characteristic of proline-containing peptides that allows for the formation of *cis* and *trans* peptide bonds as a potential strong "conformational signal" triggered by the peptide–cation interaction. Indeed, Seebach and co-workers reported ion-induced conformational effects on peptide structure to be especially pronounced in the proximity of proline.[8] Kunz et al. investigated a systematic series of proline-containing peptides using NMR spectroscopy and found that peptides containing an Asp–Pro sequence exhibit *cis*/*trans* ratios that are in opposition to those of all other sequences studied.[19] Therefore, we investigated the sequence, AXPA (Figure 1D), where P is the single letter code for proline and X is either alanine (A) or aspartate (D), thus allowing us to differentiate the contribution of pure cation–backbone interactions and cation–side-chain interactions to the peptide backbone conformation. Peptides were designed so as to avoid structure-perturbing labels and the peptide termini were protected with acetyl and aminomethyl groups (Figure 1D) to embed the sequence in a protein-like chain structure, thus avoiding end-group effects, that is, zwitterion formation.

Results and Discussion

We used a combination of exhaustive conformational searches from first principles and both theoretical and experimental gas-phase IR spectroscopy. Such investigations of isolated peptides in the gas phase offer an unbiased view of structure-formation trends intrinsic to the molecule, a strategy that is successful for charged and uncharged amino acids and peptides.[20–30] By the stepwise addition of perturbing contributions, in this case, the presence of cations, we aim to determine the main contributions to protein secondary structure formation in a bottom-up approach. The success of such an approach is critically linked to the quality of the description of the potential-energy surface of the system under investigation. We employ density-functional theory (DFT) in the generalized-gradient approximation with the Perdew–Burke–Ernzerhof (PBE) functional.[31] Van der Waals dispersion interactions are included through a pairwise C_6R^{-6} term for which the C_6 coefficients are derived from the self-consistent electron density, referred to as PBE+vdW.[32] Our use of rather accurate, but computationally-efficient approximate DFT is justified by the high-level benchmarks we present in the Computational Methods Section.

Conformational analysis: The theoretical conformational analysis of the short peptide AAPA (Figure 1D) is challenging. Hypothetically, discretizing the backbone torsion angles with a 30-degree grid and assuming two possible states (*cis* and *trans*) for the peptide bonds would formally result in roughly 35 million conformations for evaluation. To deal with such a large conformational space, we resort to a exhaustive basin-hopping search of the potential-energy surfaces (PES) of conventional protein force fields (either OPLS-AA[33] or AMBER99[34]). We employ the TINKER 5 scan routine[35] in an in-house parallelized version. To achieve a reliable and parameter-free description, we then follow up with a large set (700 to 1800 per peptide–cation system) of

PBE+vdW post-relaxation calculations as a second computational step.

Figure 2 shows our results for AAPA in isolation. The lowest-energy structure of the PES, a βVI turn with a *cis* prolyl peptide bond, also has the lowest free energy in the harmonic approximation. Two alternative βVI turns are 4.5 and 8.3 kJ mol^{-1} higher in $\Delta F_{300\,K}$. The most stable conformer with a *trans* peptide bond is a βII′ turn with $\Delta E = 2.8$ kJ mol^{-1}. Harmonic free-energy contributions add a further penalty to the structure, yielding $\Delta F_{300\,K} = 8.8$ kJ mol^{-1}. In these cases, the maximum number of four backbone hydrogen bonds is formed. In a DFT study of Ac-Ala-Pro-NMe, Byun et al. also predicted a βVI turn as the most stable conformer in the gas phase.[36] A comparable βII′ turn

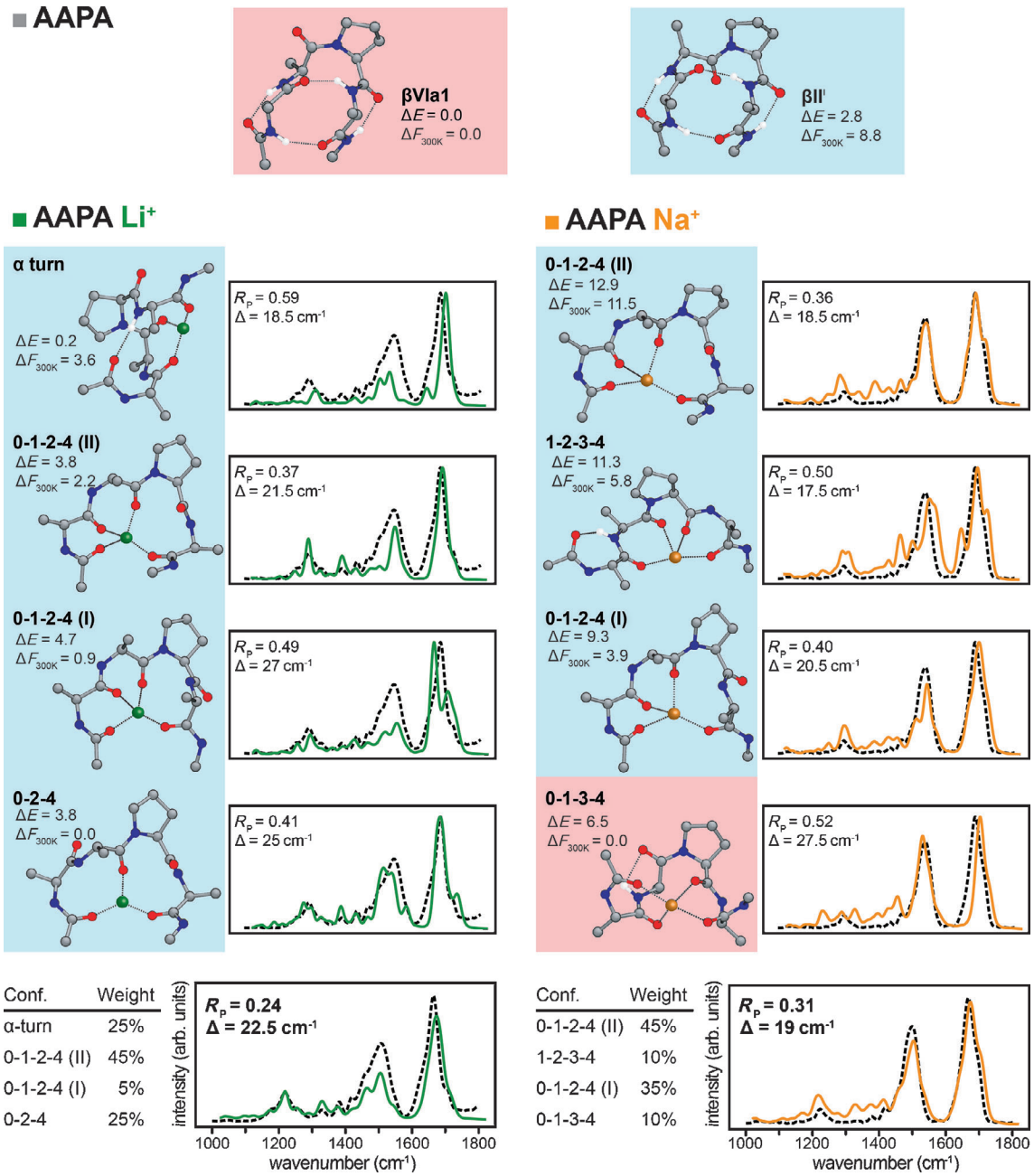

Figure 2. Low free-energy ensembles for AAPA in isolation and in the presence of Li^+ and Na^+, as obtained using exhaustive conformational searches. Potential energies (ΔE, in kJ mol^{-1}) and harmonic free energies ($\Delta F_{300\,K}$, in kJ mol^{-1}) are given. The criterion applied to select the structures shown is lowest free energy, except for conformer 0-1-2-4(II), which was selected because of its relationship with 0-1-2-4(I): both conformers can be interconverted by a backbone crankshaft movement. *Cis* and *trans* conformers are indicated using a red and blue background, respectively. The simulated IR spectra are shown as continuous lines for the individual conformers as well as for the assumed ensemble of conformers (lowest row); the experimental IR spectra are shown as dashed lines. The tables show the relative proportion of each conformer within the respective mixed simulated spectra. Simulated spectra were shifted along the energy axis by a value Δ for an optimal Pendry reliability factor, R_P. The atom colors: C is gray, N is blue, O is red, H is white, Li is green, and Na is orange. Hydrogen atoms are omitted for clarity except where they form part of a hydrogen bond.

was not among the lower-energy conformers of this shorter peptide. The lowest minima of the PES of ADPA (up to 0.7 kJ mol^{-1}) are again βVI turns (Figure 3); the next lowest in energy are two other conformers with relative potential energies of 2 and 4 kJ mol^{-1}. For the conformer that is 4 kJ mol^{-1} higher than the lowest energy conformer, the Asp side chain forms hydrogen bonds with the NH and C=O groups of residue Ala4; this conformer resembles the shape of a β turn, hence we refer to it as SC-β. For the ADPA–cation systems, we confirmed by mass spectrometry (for the ADPA–cation systems) that the Asp side chain is protonated in our experimental setup. Consequently, the Asp side chain is modeled in the protonated neutral state. Harmonic free-energy contributions make SC-β the preferred structure type by approximately 2 kJ mol^{-1}. Notably, the lowest free-energy structure of AAPA features a *cis* prolyl peptide bond, whereas the respective bond in the lowest free-energy structure of ADPA is *trans* configured (Figures 2 and 3).

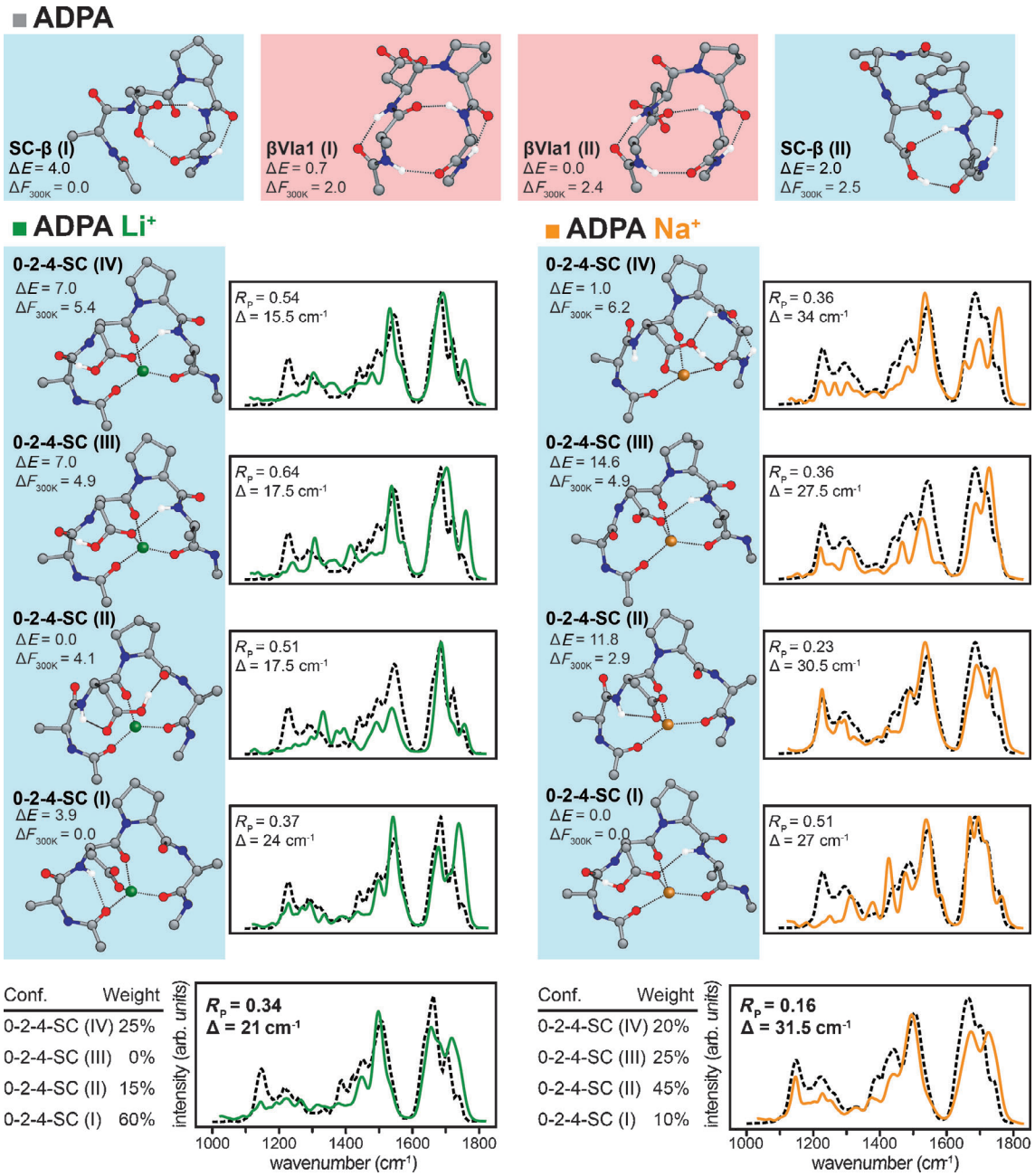

Figure 3. Low free-energy conformers of peptide ADPA in isolation and in the presence of Li^+ and Na^+. Potential energies (ΔE, in kJ mol^{-1}) and harmonic free energies ($\Delta F_{300\,K}$, in kJ mol^{-1}) are given. *Cis* and *trans* conformers are indicated using a red and blue background, respectively. The experimental and simulated IR spectra are shown as dashed and continuous lines, respectively. The simulated spectra were mixed to account for a conformational ensemble (lowest row). The tables show the relative proportion of the conformers within the mixed spectra. Simulated spectra were shifted by a value Δ along the energy axis for an optimal Pendry reliability factor, R_P. The atom colors: C is gray, N is blue, O is red, H is white, Li is green, and Na is orange. Hydrogen atoms are omitted for clarity except where they form part of a hydrogen bond.

The attraction between backbone carbonyl groups and either Li^+ or Na^+ induces structures that differ substantially from the conformers in the absence of such cations: The hydrogen-bonding networks in the low-energy conformers are disrupted (Figures 2 and 3) and the backbone conformations deviate from those of the isolated peptide. This finding is in line with the above-mentioned results for CysA in apolar Li salt solutions[5,6] and the sodiated peptide-based catalyst in the gas phase.[7] For isolated peptides AAPA and ADPA, the backbone torsion angles ϕ and ψ of the low free-energy conformers ($\Delta F_{300\,K} < 6\,kJ\,mol^{-1}$) are within the allowed regions of the Ramachandran plot (Figure 4). The single outlier in the fourth quadrant of the plot for ADPA represents the C-terminal residue, Ala4, of a conformer with $\Delta F_{300\,K} = 4.8\,kJ\,mol^{-1}$. The different possible rotameric states of the Asp side chain prefer different backbone conformations. This leads to more possible backbone conformations (data points) compared to AAPA. The cation–peptide interaction imprints ϕ/ψ combinations (backbone conformations) that differ substantially from those of the unperturbed peptides. Some of them with still low relative free-energy values ($0.9\,kJ\,mol^{-1}$ for AAPA + Li^+ to $2.6\,kJ\,mol^{-1}$ for AAPA + Na^+) are even located outside of the allowed regions of the Ramachandran plot (Figure 4). These outliers do not represent residues at the termini but rather central residues Ala2 or Asp2, which govern the overall structure of the peptides. Interestingly, the cation effects on the two peptides differ. The conformational ensembles of AAPA with Li^+ and Na^+ are different (Figures 2 and 4), whereas those of lithiated and sodiated ADPA are very similar (Figures 3 and 4).

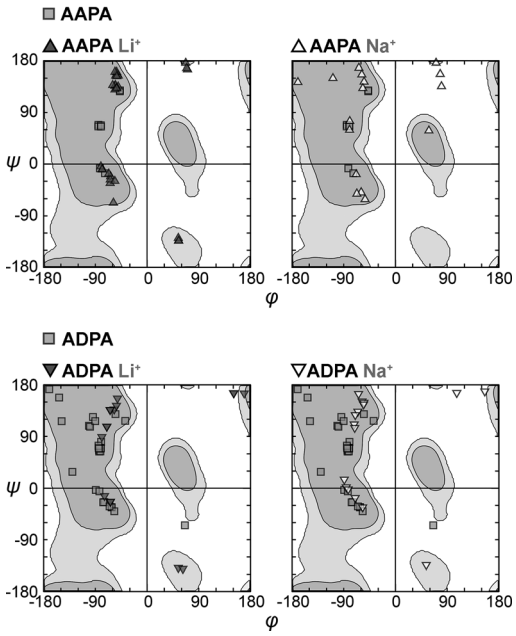

Figure 4. The backbone torsion angles, φ and ψ, of the low free-energy conformers ($\Delta F_{300\,K} < 6\,kJ\,mol^{-1}$) for AAPA and ADPA in isolation (light-gray squares), with Li^+ (dark-gray triangles), and with Na^+ (white triangles) were plotted on top of an empirical contour plot (ref. [10]).

A canonical turn structure, type βII′ (not shown), is the lowest PES minimum of AAPA + Li^+. The second most stable minimum, with $\Delta E = 0.2\,kJ\,mol^{-1}$, is an α turn (Figure 2). Here, the consideration of harmonic free-energy contributions changes the picture dramatically and unusual backbone conformations become dominant. In the lowest free-energy conformer, the Li^+ ion is coordinated by three backbone carbonyl groups of residues 0, 2, and 4 (Figure 2). The conformers resulting form the peptide–cation interactions are named according to the numbers of the interacting oxygen atoms; for example, 0-2-4. In cases of multiple conformations with the same interaction pattern, these are distinguished by roman numerals, which increase in line with the free energy of the conformers. Up to four out of a possible of five binding partners (backbone carbonyl groups) are sterically possible (conformers 0-1-2-4 with $\Delta F_{300\,K} = 0.9$ or $2.2\,kJ\,mol^{-1}$). Although the search for minima does not yield information on the actual barriers connecting different conformers, their high structural similarity suggests dynamic interconversion at a finite temperature. For AAPA + Li^+, the preferred conformation of the prolyl-peptide bond changes from *cis* to *trans*.

Na^+ binding to AAPA results in a similar behavior: canonical structure types (βVI, βII′, α) are lowest in potential energy whereas structures with both unusual backbone conformations and carbonyl groups pointing towards Na^+ are most stable when harmonic free-energy contributions are considered. However, there are substantial differences between the Na^+ and Li^+ adducts: the low free-energy ensemble of the former is more diverse and the central peptide bond of the lowest free-energy conformer 0-1-3-4 is *cis*. In the case of AAPA + Na^+, the second lowest free energy conformer (A1661, ′Delta′F 300K = 2.6 kJ mol-1) is not shown in Figure 2. This conformer was ruled out because it was proven unstable in the subsequent AIMD simulations for IR spectra (see section below). Please refer to the Supporting Information for all calculated free energies. Instead, we consider 0-1-2-4(II) as fourth conformer, which is much higher in free energy. Interestingly, these two conformers of AAPA + Na^+, 0-1-2-4(I) and 0-1-2-4(II), are almost identical other than the orientation of the peptide bond between Pro3 and Ala4 (Figure 2). This peptide bond is not involved in any interactions and can thus rotate by a concerted motion of adjacent torsion angles ψ and ϕ, a so-called backbone crankshaft rotation.[37,38] During the equilibration AIMD simulations at 300 K, which were carried out in preparation for the simulations to obtain IR spectra, this interconversion between 0-1-2-4(I) and 0-1-2-4(II) was indeed observed within the 10 ps simulation time. The subsequent evaluation of IR spectra also suggests the presence of 0-1-2-4(II) in the experimentally observed conformational ensemble.

In ADPA, the dominant interaction pattern is the complexation of either Li^+ or Na^+ by the backbone oxygen atoms 0, 2, 4 and the Asp side-chain carboxyl group. All conformers in the low-energy range are highly similar and feature no *cis* prolyl peptide bonds (Figure 3). As discussed

above on the basis of the Ramachandran plot (Figure 4), the effects of the cations on AAPA and ADPA differ. Li^+ enforces a *trans* conformation of the prolyl peptide bond of AAPA whereas Na^+ enforces the *cis* conformation (Figure 2). For ADPA, no such selectivity for the cation is observed. With either Li^+ or Na^+ attached, similar structure types with *trans* prolyl peptide bonds are preferred (Figures 3 and 4).

Infrared spectroscopy: To corroborate our structural findings, we obtained gas-phase infrared multi-photon dissociation (IRMPD) spectra, which reflect the same clean-room conditions as used in our simulations. Spectra were recorded from 1000 to 1800 cm^{-1} at the free electron laser facility FELIX[39] using a Fourier-transform ion cyclotron (FT-ICR) mass spectrometer.[40] The experimentally obtained spectra for lithiated and sodiated AAPA and ADPA are shown in Figure 2 and Figure 3. For AAPA, significantly different spectral signatures were obtained for the Li^+ and Na^+ complexed forms, a result that is in line with the results of the conformational analysis described in the previous section. On the other hand, for ADPA, very similar spectra were recorded for both cation complexes.

To allow for a quantitative theory–experiment comparison, IR spectra including anharmonic effects were computed from Born–Oppenheimer ab initio molecular dynamics (AIMD) simulations. The systems were equilibrated using 10 ps of AIMD simulations at 300 K. Subsequently, the microcanonical ensemble was sampled using up to 40 ps long AIMD simulations at constant energy from which IR spectra were derived.[41,27] IR spectra of polyamides feature characteristic bands of high intensity (like the amide I and II regions, 1400–1700 cm^{-1}) but also regions with low intensity (below 1400 cm^{-1}) and fingerprint characteristics. Visual inspection does not allow for a quantitative assessment and is, similar to a simple square of intensity comparison, easily biased by the high-intensity peaks. For a quantitative comparison between the calculated and experimental spectra, we employed the reliability factor R_P, which was introduced by Pendry to the field of low-energy electron diffraction,[42] and an implementation described by Blum and Heinz.[43] For R_P, peak positions are more important than peak intensities, a characteristic that fits the requirements we face herein, especially because we are comparing experimental action spectra and theoretical absorption spectra. Values for R_P range from 0 (perfect agreement) to 1 (no correlation). Intensities of the spectra were normalized to 1 and rigidly shifted (not scaled) with a value Δ along the energy axis to account for deviations owing to a systematic mode softening by the density functional we use.[44,27] When comparing the calculated IR spectra of single conformations to the experimental IR spectra we observe only modest agreement (see individual spectra in Figures 2 and 3). Previous studies have shown similar behavior owing to conformational ensembles for peptides in the gas phase at finite temperature.[22–27] Furthermore, the energy differences of the low free-energy conformers lie within the uncertainty of the employed method, as discussed in the section called 'Benchmarks' below. Consequently, an ensemble of conformations is assumed. By mixing the individual theoretical spectra in 5% steps, the R_P for the respective experimental spectrum is optimized. This results in a much better agreement of simulated and experimental spectra of the peptides AAPA and ADPA in complex with single Li^+ or Na^+ ions (Figures 2 and 3). The agreement between predicted and experimental spectra of $AAPA+Li^+$ and $ADPA+Li^+$ and between those of the corresponding complexes of Na^+, especially regarding the fine structure below 1400 cm^{-1}, is gratifying. We note for completeness that the spectra for the protonated peptides (not shown) are rather different in appearance, suggesting very different structural effects compared to those induced by the presence of heavier cations.

In a naive way, a correlation between the free-energy estimates in the harmonic approximation and the abundances of the individual spectra in the resulting mixed spectrum could be expected. However, this would be too much to expect for several reasons:

(1) The PBE+vdW method we use is rather accurate as illustrated by the benchmark calculation presented below; however, the systems under investigation here are also large (56 to 60 atoms). The lowest free-energy minima discussed herein are still within the range of uncertainty in the values of the relative (free) energies.
(2) The experimental data base which we are comparing to multiple theoretical spectra is relatively small; fitting many parameters to a small data set has well known limitations.[42] The use of multiple spectra, therefore, is strictly only a consistency check. The spectra of just a single conformer are not sufficient to explain the observed IR spectra. In contrast, the use of spectra of multiple conformers yield a much more consistent description of the spectra, in line with several conformers of similar free energy. This is the primary qualitative statement that we can derive from the experiment–theory comparison.
(3) The here employed free-energy model neglects anharmonicity as well as the entropic effects of a possibly greater accessible conformational space (dynamic interconversion in the case of low barriers) of specific conformers. That the latter can be of special importance is illustrated by the crankshaft rotation discussed above for the two conformers, 0-1-2-4(I) and 0-1-2-4(II) of $AAPA+Na^+$. That both conformers can interconvert shows the extent to which the anharmonic nature of the potential-energy surface can play a role. In fact, in the combination of the four individual spectra that shows the best agreement with the experimental spectrum (Figure 2), 0-1-2-4(II) is the predominant conformer with 45% of the total population of the species. Again, conformer 0-1-2-4(II) is structurally and dynamically closely related to the 0-1-2-4(I) conformer with the lowest harmonic free energy. This result illustrates the limits of the harmonic free-energy assignment to poten-

tial-energy minima at room temperature, which neglects such conformational and dynamical effects. The result furthermore illustrates the limitations of interpreting IR spectra by using a combination of individual and isolated conformers.

Overall, on the one hand, the accuracy of the harmonic approximation to the free energy is limited by the dynamic character of such molecular systems at finite temperature; on the other hand, the IRMPD spectroscopy setup we use here is limited in its resolution, especially regarding the separation of individual conformers. However, we can unambiguously predict minima by first-principles theory and validate the results by room-temperature IR spectroscopy (keeping the differences of static harmonic free-energy minima and actual room-temperature molecules in mind). The observed cation–peptide effects were certainly qualitatively corroborated by both approaches.

Microsolvation of a peptide–cation complex: In the introduction, we mentioned the presence of turn sequences, which are mainly located at the surface of proteins and thus exposed to the aqueous environment. In this section, a qualitative picture of how the interaction between the peptide backbone and the cation can compete with solvation of the cation is given. AIMD simulations were performed for AAPA+Li^+ alone and with a few water molecules. For the setup of the latter system, 18 water molecules were accommodated within a sphere of radius 4.5 Å around the Li^+ ion. For comparison, Li^+ embedded within both 4 and 10 water molecules was also studied. We characterized the interaction between the Li^+ ion and either the respective oxygen atoms of the peptide backbone or of first-solvation-shell water molecules by the Li^+–O distance and by the O–Li^+–O angle (Figure 5). Previous ab initio studies predict a coordination number of 4 for Li^+ in water.[23,45,46] Consistent with these studies, the cation is complexed by 4 backbone carbonyl groups in, for example, conformer 0-1-2-4(I). During a 100 ps AIMD trajectory at 330 K (Nosé–Hoover thermostat), the Li^+–O distance fluctuates around 1.9 Å, the O-Li^+-O angle distribution is broad, thus indicating the nonideal tetrahedron formed by the interacting carbonyl oxygen atoms. The microsolvation of AAPA+Li^+ within 18 water molecules results in a slight change of the binding site within a few picoseconds: a water oxygen atom substitutes for the backbone C=O group of Ala1. The cation interacts with the three backbone carbonyl oxygen atoms of AAPA and the same water molecule (Figure 5) for the whole 90 ps of remaining AIMD simulation time. As a result, a virtually ideal binding site is formed, characterized by an almost symmetric distribution of the O-Li^+-O angle around the ideal tetrahedral angle of 109.5°. For Li^+ immersed within a small water cluster (either 4 or 10 water molecules), the Li^+–O distance distribution peaks around 2.0 Å. Remarkably, the distribution of the tetrahedron angles O-Li^+-O is multimodal again, accounting for alternative (and less populated) geometries of the Li^+ complex involving 3 or, in the case of the 10 water molecules with Li^+ cluster, even 5 water molecules in the first solvation shell. For now, we can at least qualitatively say that AAPA is able to form an ideal interaction shell that seems to be able to compete with water solvation. A fully correct answer could be given on the basis of free-energy differences from simulations with fully solvated systems. Such simulations are standard for force-field approaches, yet they are computationally very demanding at the level of theory we employ here. A rigorous assessment is thus beyond the scope of this article.

Conclusion

Starting from the isolated peptides that adopt either canonical turn structures (AAPA) or turn-like conformations with hydrogen bonds between the side chains and the backbones (ADPA), we show the drastic effect of cations on the local

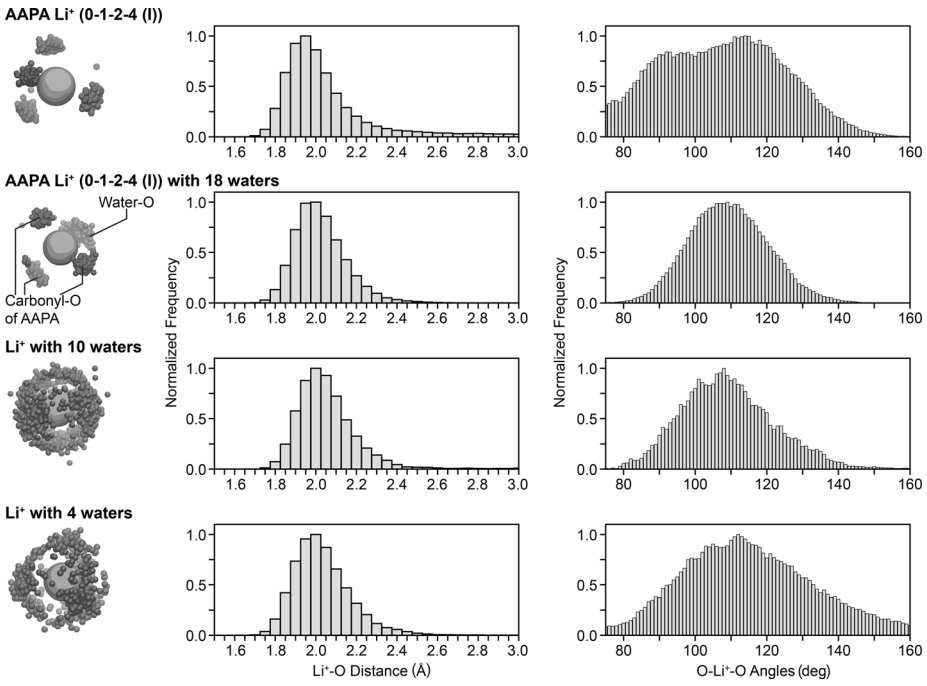

Figure 5. The first solvation shell around a Li^+ ion. Interactions are formed with the oxygen atoms of water molecules or those of backbone carbonyl groups. The histograms were derived from AIMD simulation of different length (20 to 100 ps) and the counts were normalized to 1.

secondary structure of peptides: the cation interacts with most of the backbone carbonyl groups and, as a result, completely breaks the local hydrogen-bonding network. This leads to distortions of the peptide backbone and results in conformations with backbone torsion angles ϕ and ψ that are, in part, outside of the allowed regions of the Ramachandran plot (Figure 4). Consequently the question of the range of such ion-induced disruptions arises. Ohanessian and co-workers studied[47,48] polyglycines with a chain length of 2 to 8 residues in complex with Na^+ by simulation and gas-phase IR spectroscopy: for sequences of up to 7 glycine residues, the contact number between the cation and backbone C=O groups is maximized and no hydrogen bonding was observed. With the Gly_8 peptide, backbone hydrogen bonding appeared again in the form of γ- and β turns. Glycine, owing to the lack of a side chain, is a very special case among the canonical amino acids. As a contrast, the helical secondary structure of sodiated polyalanine (8–12 residues) is not broken in the gas phase. Here, the Na^+ ion is attached to the C terminus.[49,50] The importance of considering the effect of side-chain functionalities is highlighted by the sequence dependence of the cation effects we observe. The conformational preferences of AAPA with either Li^+ or Na^+ differ drastically in the *trans*/*cis* state of the central prolyl peptide bond. Noskov and Roux investigated the selectivity of the ion-coupled transporter LeuT. Two Na^+ binding sites (NA1 and NA2) show differences in the Li^+/Na^+ selectivity: NA1 appears to be rather flexible and exhibits no selectivity for one cation over the other as it adapts to the different ionic radii; for NA2, a limited selectivity is apparently induced by a "snug-fit" mechanism (the rigid NA2 interaction site is unable to adapt to different ionic radii).[51] Similarly, lowest free-energy structure 0-1-3-4 of AAPA + Na^+ may be too rigid to adapt to the Li^+ cation, because only backbone carbonyl groups can be involved in the interaction. With ADPA, the Asp side chain prevents such conformation selectivity.

Our findings might even help to understand a basic biochemical principle: in 1888, Hofmeister published an article[52] that laid the basis for a sorting of cations and anions according to their effect on the solubility of biomolecules, colloids, and functional polymers. Although it was believed that the underlying effects can be explained solely by bulk properties stemming from the solvent–ion interactions,[53] evidence was found that most effects of ions on water structure are limited to the first solvation shell[54] and that specific ion–solute interactions can be expected to contribute substantially.[55] These effects are especially clear at high salt concentrations as shown by Dzubiella and co-workers, who employed classical MD simulations,[56–58] and later, experimental approaches.[59] They demonstrated that the perturbing effect of ions on peptide structure results from the breaking of secondary-structure-specific hydrogen bonds in the backbone. Our own findings point to a similar direction, as we have shown here how cations can substantially change the backbone structure of a (bio)polymer. These interactions are not necessarily stable over a very long time range, but our exploratory AIMD simulations suggest time ranges at least in the tens to hundreds of picoseconds. Dzubiella described long-lived loop conformations that are stable over 10 to 20 ns in classical MD trajectories.[56] Similar to the specific interactions between anions and the amide-bond-containing polymers of *N*-isopropylacrylamide described by Cremer and co-workers,[60] we show here the possible interactions between small monovalent cations and peptides and highlight their significant effect on local peptide structure. These effects could be one of the drivers behind the Hofmeister salt effects on proteins.

Computational methods

Scans of the PES were performed with an exhaustive basin-hopping search and conventional protein force fields (either OPLS-AA[33] or AMBER99[34]). We employ the TINKER 5 scan routine[35] in an in-house parallelized version. The required methods to perform DFT-based simulations, including geometry optimization, computation of harmonic vibrations, and ab initio Born–Oppenheimer molecular dynamics (AIMD), are incorporated in the FHI-aims code, which provides an efficient and accurate all-electron description based on numeric atom-centered orbitals.[61] We discuss fully relaxed conformations at the PBE+vdW level and their relative potential energies (ΔE) and relative harmonic free energies at 300 K ($\Delta F_{300\,K}$), all computed with tight convergence settings and an accurate tier-2 basis set.[61] High-level quantum-chemical benchmark calculations, that is, relaxations at the MP2 level of theory and coupled-cluster calculations with singles, doubles, and perturbative triples (CCSD(T)), were performed with the ORCA quantum-chemistry program;[62] CCSD(T) energies extrapolated to the complete basis-set limit (CBS) were obtained by a method described by Truhlar,[63] employing the Dunning basis sets cc-pVDZ and cc-pVTZ.[64]

Benchmarks: We assessed the predictive power of the DFT approximations applied here by benchmarks in two directions with respect to the approximation level: we compare these approximations to high-level quantum-chemistry calculations at the CCSD(T) level of theory extrapolated to the complete basis-set limit. On the other hand, we assess the quality of the force-field description of cation–peptide interactions in comparison to approximate DFT at the PBE+vdW and PBE0+vdW levels.

Comparing electronic-structure theory methods: There have been several assessments of the accuracy of the PBE+vdW level of theory applied to a variety of systems, such as peptides,[65] weakly bound metal–phtalocyanine systems,[66] and ionic and semiconductor solids.[67] A previous assessment of the accuracy of PBE+vdW level of theory for peptide systems, for the conformational-energy hierarchy of Ace-Ala-NMe and Ace-Ala_3-NMe, shows mean absolute errors (MAE) below 2 kJ mol^{-1} in comparison to CCSD(T) energies.[65] Herein, we investigate cation–peptide systems and thus reassess the accuracy of our DFT-based predictions. We employ high-level quantum chemical theory on the conformational-energy hierarchy of Ac-Ala-NMe + Li^+. A conformational analysis identified five local minima (Figure 6) within a potential-energy range of 35 kJ mol^{-1} at the MP2/cc-pVTZ level of theory.[64,68] The cation closes a 7-membered pseudocycle through interaction with the oxygen atoms of the backbone carbonyl groups. The orientation of the methyl groups relative to the pseudocycle plane defines them as either equatorial (Figure 6; **1**, **3**, **5**) or axial (Figure 6; **2**, **4**). In addition, an important characteristic of our actual systems of interest (AAPA and ADPA) is present here as well: in lower-energy conformers **1** and **2**, the C-terminal peptide bond is *trans* configured, which is in contrast to the other conformers with a C-terminal *cis* peptide bond.

Relative energies at the CCSD(T), PBE+vdW, and PBE0+vdW levels of theory were compared by estimating the mean absolute error ($\mathrm{MAE} = \frac{1}{n}\sum_{i=1}^{n} |f_i - y_i|$). As an additional method, we also include the

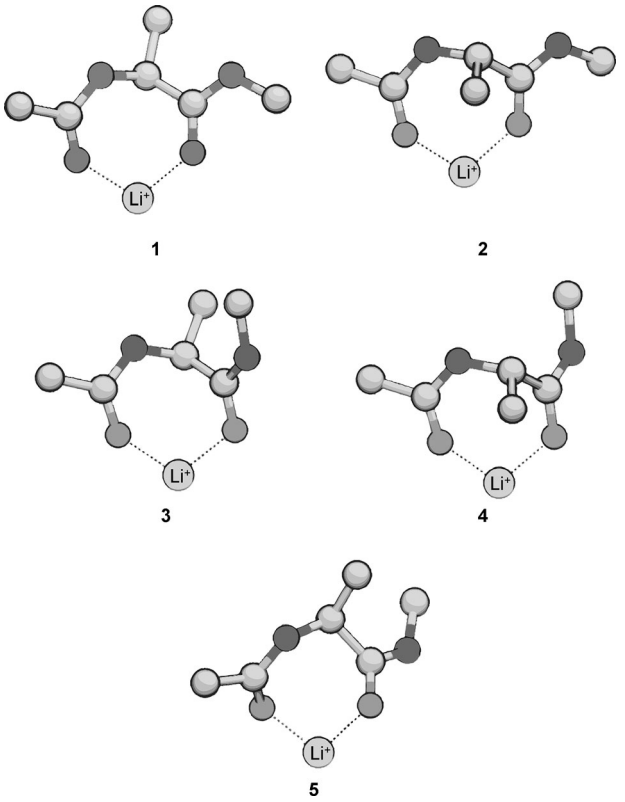

Figure 6. Lowest-energy conformers of Ace-Ala-NHMe+Li^+, fully relaxed at the MP2/cc-pVTZ level of ab initio theory. Hydrogen atoms were omitted for clarity; dashed black lines show the oxygen–lithium interactions.

frequently used B3LYP method (no vdW correction). For much larger systems, the missing description of dispersion effects represents a deficiency in the description of conformational-energy hierarchies. The DFT methods give low uncertainties (see Table 1), well within the often stressed "chemical accuracy" of 1 kcal mol^{-1} (4.2 kJ mol^{-1}). The conformational changes upon relaxation with DFT are negligible, as indicated by the low maximal RMSD value of 0.38 Å (Table 1). We note that only small contributions of the van der Waals correction can be expected for molecular systems of this size. Of the tested DFT approaches, PBE0+vdW gives the best agreement with the benchmark calculations, as it is obvious from the MAE and the average RMSD (see Table 1). However, for a large-scale conformational screening and the extensive molecular dynamics simulations we undertake in this study, PBE+vdW strikes a perfect balance between computational cost and accuracy.

Standard protein force fields versus electronic structure theory: When comparing the results of different standard protein force fields and DFT, we observe dramatic discrepancies in the conformational hierarchies. Such force fields were parameterized for the solvated state, whereas our assessment was based in the gas phase. Nonetheless, these force fields are also frequently used for conformational investigations irrespective of the environment. Consequently, their performance in vacuo is of interest. As a reference, we employ the conformational-energy hierarchy of AAPA+Li^+ at the PBE+vdW level. In line with the results of the above comparison, PBE[31] and the hybrid density functional, PBE0,[69] (both vdW corrected)[32] give very similar results, illustrated by the low mean absolute (MAE) and maximal errors (E_{max}) listed in Table 2. Both approaches without the vdW correction give higher values for MAE and E_{max}. The widely used protein force fields, Amber99,[34] Charmm22,[70] and OPLS-AA,[33] give MAE values that are at least approximately 15 times larger and very large E_{max} values (see Table 2). The relative energies can be found in the Supporting Information. The main characteristic of the system is apparently the cation–peptide interaction. The effect on the partial charges appears to be better described by the polarizable FF Amoeba,[71] illustrated by a MAE value of about 10 kJ mol^{-1}. The removal of the cation leads to reduced MAE values for the FF methods (see Table 2); also, the energy hierarchies themselves appear more consistent among the different methods. This is apparent either when comparing the two plots (in the presence and absence of Li^+) in Figure 7 or when studying the maximal error values, as given in Table 2. The calculations (single point) were repeated for the same AAPA conformers (fixed geometries) but without the cation. The MAE values obtained using the force-field approaches are consistently much larger than those obtained using the DFT techniques, with significant errors in the energetic hierarchy of the conformers. Apparently, the large errors of the force fields can mainly be attributed to the ill-described cation–peptide interaction. In short, DFT-based approaches for cation–peptide systems appear to be superior to standard force field based approaches tested here.

Table 1. Relative energies and RMSD values of the conformers depicted in Figure 6.[a]

	E (MP2 geometries)				RMSD to MP2		
Conf.	CCSD(T)	PBE+vdW	PBE0+vdW	B3LYP	PBE+vdW	PBE0+vdW	B3LYP
1	0.0	0.0	0.0	0.0	0.03	0.03	0.03
2	6.7	4.4	5.0	5.7	0.03	0.03	0.03
3	20.2	17.1	18.2	22.3	0.38	0.16	0.33
4	23.1	22.0	23.1	27.1	0.12	0.08	0.18
5	33.8	34.2	34.8	38.0	0.04	0.02	0.04
MAE/RMSD		1.4	0.9	2.3	0.12	0.06	0.12

[a] Left columns: CCSD(T), PBE+vdW, PBE0+vdW, and B3LYP relative energies were calculated for MP2/cc-pVTZ geometries. The MAE of the DFT relative-energy hierarchies to CCSD(T) is also given. Right columns: the conformers were also relaxed with the respective DFT methods. With respect to the MP2 geometries, RMSD values for the individual conformers and average RMSD values are given. Relative energies and the mean absolute error (MAE) values are given in kJ mol^{-1}; RMSD values are given in Å.

Experimental methods

Synthesis: Peptides were synthesized by solid-phase assembly using a Multi-Syntech Syro XP peptide synthesizer (MultisynTech GmbH, Witten, Germany) and an Fmoc strategy on Fmoc-Ala-OWang resin (0.5 mmol g^{-1}). The peptides were cleaved from the resin by reaction with 2 mL of a solution containing 10% (*w*/*v*) triisopropylsilane, 1% (*w*/*v*) water, and 89% (*w*/*v*) trifluoroacetic acid (TFA). The crude peptides were purified by reversed-phase HPLC on a Knauer smartline manager 5000 system (Knauer, Berlin, Germany) equipped with a C8 (10 μm) LUNATM Phenomenex column (Phenomenex, Torrance, CA, USA). Peptides were eluted with a linear gradient of acetonitrile/water/0.1% TFA and identified on an Agilent 6210 ESI-TOF mass spectrometer. Peptide purity was determined by analytical HPLC on a Merck LaChrom system (Merck KGaA, Darmstadt, Germany) equipped with a C8 (10 μm) LUNATM Phenomenex column (Phenomenex, Torrance, CA, USA). The gradient used was similar to those used for the preparative HPLC.

Infrared spectroscopy: The gas-phase IR experiments were performed at the free electron laser facility FELIX[39] (Nieuwegein, The Netherlands) using the Fourier-transform ion cyclotron (FT-ICR) mass spectrometer[40] which was temporarily equipped with a nano electrospray ionization (nESI) source (MS Vision, Almere, The Netherlands). Typically, 5 μL of a solution

Table 2. MAE and E_{max} values.[a]

	PBE0+vdW	PBE	PBE0	Amoeba	Amber99	Charmm22	OPLS-AA
	Fixed AAPA+Li^+ geometries						
MAE	1.0	5.7	6.1	9.7	15.7	20.5	26.0
E_{max}	2.0	10.9	11.1	22.3	30.1	53.6	69.1
	Same geometries, fixed without Li^+						
MAE	1.1	6.6	6.6	8.1	14.0	15.6	11.6
E_{max}	2.8	14.3	14.8	20.3	37.5	36.8	29.7

[a] MAE and E_{max} values with respect to the PBE+vdW hierarchy, of the energy hierarchies computed with PBE0+vdW, PBE, PBE0, Amoeba (ref. [71]), Amber99 (ref. [34]), Charmm22 (ref. [70]), and OPLS (ref. [33]) for the fixed geometries of AAPA with and without the Li^+ ion (energies in kJ mol^{-1}). The relative energies can be found in Tables 1 and 2 of the Supporting Information.

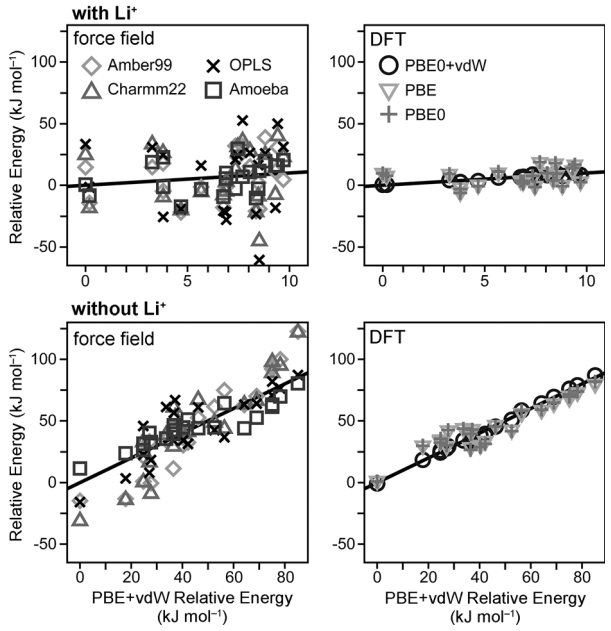

Figure 7. The relative energies of 21 AAPA+Li^+ conformers with a relative potential energy below 10 kJ mol^{-1} at the PBE+vdW level were recalculated with PBE0+vdW, PBE, PBE0, Amoeba (ref. [71]), Amber99 (ref. [34]), Charmm22 (ref. [70]), and OPLS (ref. [33]) for the fixed geometries with and without the Li^+ ion. The conformational energy hierarchies with different FF and DFT methods are plotted against the PBE+vdW values (*x* axis). The relative energy values were shifted according to the overall offset of the individual energy hierarchy. Please note the different scales of the *x* axes in the plots with and without Li^+ cation. The hypothetical perfect correlation is indicated by the straight lines.

containing 1 mM peptide, 50% water, 50% methanol and, where needed, 10 mM LiCl or NaCl, were placed in gold-coated off-line emitters prepared in-house. To obtain a stable spray, a small backing pressure of approximately 0.5 bar and a relatively low capillary voltage of approximately 850 V was applied to the needle. The nESI-generated ions were accumulated in a hexapole ion trap and subsequently transferred into the FT-ICR mass spectrometer that is optically accessible through a KRS-5 window at the back end. After trapping and SWIFT mass isolation inside the ICR cell, the ions were irradiated by IR photons of the free electron laser FELIX.[72] The light provided by FELIX consists of macropulses of about 5 μs length at a repetition rate of 10 Hz, which contain 0.3 to 5 ps long micropulses with a micropulse spacing of 1 ns. The wavelength is continuously tunable over a range of 40 to 2000 cm^{-1}. Here, typically wavelengths from 500 to 1850 cm^{-1} were scanned. When the IR light is resonant with an IR-active vibrational mode in the molecule, this results in the absorption of many photons, thus causing dissociation of the ion (IRMPD). Monitoring of the fragmentation yield as a function of IR wavelength leads to the IR spectra.

Acknowledgements

The authors acknowledge continuous interest and support from Gerard Meijer (Radboud University Nijmegen). We gratefully acknowledge the "Stichting voor Fundamenteel Onderzoek der Materie" (FOM) for providing the beam time on FELIX as well as the support of the FELIX staff: Britta Redlich, Lex van der Meer, Rene van Buuren, Jos Oomens, Giel Berden, and Josipa Grzetic. Franziska Schubert, Sucismita Chutia, and Mariana Rossi (FHI Berlin) are acknowledged for discussion and technical help. C. B. is grateful to Hans-Jörg Hofmann (Universität Leipzig) for inspiring discussions.

[1] P. Pfeiffer, J. von Modelski, *Hoppe-Seylers Z. Physiol. Chem.* **1912**, *81*, 329–354.
[2] P. Pfeiffer, *Hoppe-Seylers Z. Physiol. Chem.* **1924**, *133*, 22–61.
[3] D. Seebach, H. Bossler, R. Flowers, E. Arnett, *Helv. Chim. Acta* **1994**, *77*, 291–305.
[4] J. Kofron, P. Kuzmič, V. Kishore, E. Colón-Bonilla, D. Rich, *Biochemistry* **1991**, *30*, 6127–6134.
[5] H. Kessler, M. Gehrke, J. Lautz, M. Kock, D. Seebach, A. Thaler, *Biochem Pharmacol.* **1990**, *40*, 169–173.
[6] M. Koeck, H. Kessler, D. Seebach, A. Thaler, *J. Am. Chem. Soc.* **1992**, *114*, 2676–2686.
[7] E. Garand, M. Z. Kamrath, P. A. Jordan, A. B. Wolk, C. M. Leavitt, A. B. McCoy, S. J. Miller, M. A. Johnson, *Science* **2012**, *335*, 694–698.
[8] D. Seebach, A. K. Beck, A. Studer in *Modern Synthetic Methods* (Eds.: B. Ernst, C Leumann), Wiley-VCH, **1995**; pp. 1–178.
[9] G. Ramachandran, C. Ramakrishnan, V. Sasisekharan, *J. Mol. Biol.* **1963**, *7*, 95–99.
[10] S. C. Lovell, I. W. Davis, W. B. Arendall, P. I. W. de Bakker, J. M. Word, M. G. Prisant, J. S. Richardson, D. C. Richardson, *Proteins: Struct. Funct. Bioinf.* **2003**, *50*, 437–450.
[11] G. Fischer, *Chem. Soc. Rev.* **2000**, *29*, 119–127.
[12] C. Dugave, L. Demange, *Chem. Rev.* **2003**, *103*, 2475–2532.
[13] M. S. Weiss, A. Jabs, R. Hilgenfeld, *Nat. Struct. Biol.* **1998**, *5*, 676–676.
[14] J. S. Richardson, *Adv. Protein Chem.* **1981**, *34*, 167–339.
[15] For idealized backbone torsion angles for these turn types, see: K. Möhle, M. Gußmann, H.-J. Hofmann, *J. Comput. Chem.* **1997**, *18*, 1415–1430.
[16] C. M. Venkatachalam, *Biopolymers* **1968**, *6*, 1425–1436.
[17] B. L. Sibanda, J. M. Thornton, *Nature* **1985**, *316*, 170–174.
[18] E. G. Hutchinson, J. M. Thornton, *Protein Sci.* **1994**, *3*, 2207–2216.
[19] C. Kunz, G. Jahreis, R. Günther, S. Berger, G. Fischer, H.-J. Hofmann, *J. Pept. Sci.* **2012**, *18*, 400–404.
[20] A. Abo-Riziq, J. E. Bushnell, B. Crews, M. Callahan, L. Grace, M. S. de Vries, *Chem. Phys. Lett.* **2006**, *431*, 227–230.
[21] J. Bakker, L. Aleese, G. Meijer, G. von Helden, *Phys. Rev. Lett.* **2003**, *91*, 203003.
[22] I. Compagnon, J. Oomens, G. Meijer, G. von Helden, *J. Am. Chem. Soc.* **2006**, *128*, 3592–3597.
[23] A. Kamariotis, O. V. Boyarkin, S. R. Mercier, R. D. Beck, M. F. Bush, E. R. Williams, T. R. Rizzo, *J. Am. Chem. Soc.* **2006**, *128*, 905–916.
[24] A. Cimas, T. D. Vaden, T. S. J. A. de Boer, L. C. Snoek, M.-P. Gaigeot, *J. Chem. Theory Comput.* **2009**, *5*, 1068–1078.

[25] W. H. James III, C. W. Müller, E. G. Buchanan, M. G. D. Nix, L. Guo, L. Roskop, M. S. Gordon, L. V. Slipchenko, S. H. Gellman, T. S. Zwier, *J. Am. Chem. Soc.* **2009**, *131*, 14243–14245.
[26] W. H. James III, E. E. Baquero, S. H. Choi, S. H. Gellman, T. S. Zwier, *J. Phys. Chem. A* **2010**, *114*, 1581–1591.
[27] M. Rossi, V. Blum, P. Kupser, G. von Helden, F. Bierau, K. Pagel, G. Meijer, M. Scheffler, *J. Phys. Chem. Lett.* **2010**, *1*, 3465–3470.
[28] R. J. Plowright, E. Gloaguen, M. Mons, *ChemPhysChem* **2011**, *12*, 1889–1899.
[29] S. Chutia, M. Rossi, V. Blum, *J. Phys. Chem. B* **2012**, *116*, 14788–14804.
[30] M. Rossi, M. Scheffer, V. Blum, *J. Phys. Chem. B* **2013**, *117*, 5574–5584.
[31] J. P. Perdew, K. Burke, M. Ernzerhof, *Phys. Rev. Lett.* **1996**, *77*, 3865–3868.
[32] A. Tkatchenko, M. Scheffler, *Phys. Rev. Lett.* **2009**, *102*, 073005.
[33] W. Jorgensen, J. Ulmschneider, J. Tirado-Rives, *J. Phys. Chem. B* **2004**, *108*, 16264–16270.
[34] J. Wang, P. Cieplak, P. Kollman, *J. Comput. Chem.* **2000**, *21*, 1049–1074.
[35] R. Pappu, R. Hart, J. Ponder, *J. Phys. Chem. B* **1998**, *102*, 9725–9742.
[36] B. Byun, I. Song, Y. Chung, K. Ryu, Y. Kang, *J. Phys. Chem. B* **2010**, *114*, 14077–14086.
[37] Z. Wasserman, F. Salemme, *Biopolymers* **1990**, *29*, 1613–1631.
[38] A. R. Fadel, D. Q. Jin, G. T. Montelione, R. M. Levy, *J. Biomol. NMR* **1995**, *6*, 221–226.
[39] D. Oepts, A. van der Meer, P. van Amersfoort, *Infrared Phys. Technol.* **1995**, *36*, 297–308.
[40] J. Valle, J. Eyler, J. Oomens, D. Moore, A. van der Meer, G. von Helden, G. Meijer, C. Hendrickson, A. Marshall, G. Blakney, *Rev. Sci. Instrum.* **2005**, *76*, 023103.
[41] M.-P. Gaigeot, *Phys. Chem. Chem. Phys.* **2010**, *12*, 3336–3359.
[42] J. Pendry, *J. Phys. C: Solid State Phys* **1980**, *13*, 937–944.
[43] V. Blum, K. Heinz, *Comput. Phys. Commun.* **2001**, *134*, 392–425.
[44] G. Grégoire, M. P. Gaigeot, D. C. Marinica, J. Lemaire, J. P. Schermann, C. Desfrancois, *Phys. Chem. Chem. Phys.* **2007**, *9*, 3082–3097.
[45] S. Varma, S. B. Rempe, *Biophys. Chem.* **2006**, *124*, 192–199.
[46] T. Ikeda, M. Boero, K. Terakura, *J. Chem. Phys.* **2007**, *126*, 034501.
[47] D. Semrouni, O. P. Balaj, F. Calvo, C. F. Correia, C. Clavagura, G. Ohanessian, *J. Am. Soc. Mass Spectrom.* **2010**, *21*, 728–738.
[48] O. P. Balaj, D. Semrouni, V. Steinmetz, E. Nicol, C. Clavaguéra, G. Ohanessian, *Chem. Eur. J.* **2012**, *18*, 4583–4592.
[49] M. Kohtani, B. Kinnear, M. Jarrold, *J. Am. Chem. Soc.* **2000**, *122*, 12377–12378.
[50] J. K. Martens, I. Compagnon, E. Nicol, T. B. McMahon, C. Clavaguéra, G. Ohanessian, *J. Phys. Chem. Lett.* **2012**, *3*, 3320–3324.
[51] S. Y. Noskov, B. Roux, *J. Mol. Biol.* **2008**, *377*, 804–818.
[52] F. N.-S. Hofmeister, *Arch. Pharmakol.* **1888**, *25*, 1–30.
[53] P. H. von Hippel, K.-Y. Wong, *J. Biol. Chem.* **1965**, *240*, 3909–3923.
[54] A. W. Omta, M. F. Kropman, S. Woutersen, H. J. Bakker, *Science* **2003**, *301*, 347–349.
[55] W. Kunz, *Curr Opin. Colloid Interface Sci.* **2010**, *15*, 34–39.
[56] J. Dzubiella, *J. Am. Chem. Soc.* **2008**, *130*, 14000–14007.
[57] J. Dzubiella, *J. Phys. Chem. B* **2009**, *113*, 16689–16694.
[58] Y. von Hansen, I. Kalcher, J. Dzubiella, *J. Phys. Chem. B* **2010**, *114*, 13815–13822.
[59] A. Crevenna, N. Naredi-Rainer, D. Lamb, R. Wedlich-Söldner, J. Dzubiella, *Biophys. J.* **2012**, *102*, 907–915.
[60] Y. Zhang, S. Furyk, D. E. Bergbreiter, P. S. Cremer, *J. Am. Chem. Soc.* **2005**, *127*, 14505–14510.
[61] V. Blum, R. Gehrke, F. Hanke, P. Havu, V. Havu, X. Ren, K. Reuter, M. Scheffler, *Comput. Phys. Commun.* **2009**, *180*, 2175–2196.
[62] F. Neese, *Wiley Interdiscip. Rev.: Comput. Mol. Sci.* **2012**, *2*, 73–78.
[63] D. G. Truhlar, Chem. Phys. Lett. **1998**, *294*, 45–48.
[64] T. H. Dunning Jr., *J. Chem. Phys.* **1989**, *90*, 1007–1023.
[65] A. Tkatchenko, M. Rossi, V. Blum, J. Ireta, M. Scheffler, *Phys. Rev. Lett.* **2011**, *106*, 118102.
[66] N. Marom, A. Tkatchenko, M. Scheffler, L. Kronik, *J. Chem. Theory Comput.* **2010**, *6*, 81–90.
[67] G.-X. Zhang, A. Tkatchenko, J. Paier, H. Appel, M. Scheffler, *Phys. Rev. Lett.* **2011**, *107*, 245501.
[68] J. A. Pople, J. S. Binkley, R. Seeger, *Int. J. Quantum Chem.* **1976**, *10*, 1–19.
[69] C. Adamo, V. Barone, J. Chem. Phys. **1999**, *110*, 6158–6170.
[70] A. D. MacKerell, Jr., D. Bashford, M. Bellott, R. L. Dunbrack Jr., J. D. Evanseck, M. J. Field, S. Fischer, J. Gao, H. Guo, S. Ha, D. Joseph-McCarthy, L. Kuchnir, K. Kuczera, F. T. K. Lau, C. Mattos, S. Michnick, T. Ngo, D. T. Nguyen, B. Prodhom, W. E. Reiher III, B. Roux, M. Schlenkrich, J. C. Smith, R. Stote, J. Straub, M. Watanabe, J. Wiórkiewicz-Kuczera, D. Yin, M. Karplus, *J. Phys. Chem. B* **1998**, *102*, 3586–3616.
[71] M. Schnieders, J. Ponder, *J. Chem. Theory Comput.* **2007**, *3*, 2083–2097.
[72] J. Oomens, B. Sartakov, G. Meijer, G. von Helden, *Int. J. Mass Spectrom.* **2006**, *254*, 1–19.

Received: December 21, 2012
Published online: ■■ ▮▮, 0000

